*Journal of Thermal Analysis and Calorimetry, Vol. 88 (2007) 1, 163–169*

# THERMAL BEHAVIOUR STUDY OF SOME SOL–GEL IRON-SILICA NANOCOMPOSITES

*Ana Brăileanu*[1*], *M. Răileanu*[1], *M. Crişan*[1], *D. Crişan*[1], *R. Bîrjega*[2], *V. E. Marinescu*[3], *J. Madarász*[4] *and G. Pokol*[4]

[1]Roumanian Academy, Institute of Physical Chemistry Ilie Murgulescu, 202 Splaiul Independenţei, 060021 Bucharest, Roumania
[2]National Institute for Lasers, Plasma and Radiation Physics, PO Box MG-36, 76900 Bucharest, Roumania
[3]INCDIE ICPE-CA, 313 Spl. Unirii, 030138 Bucharest, Roumania
[4]Budapest University of Technology and Economics, Institute of General and Analytical Chemistry, Szt. Gellért tér 4 1521 Budapest, Hungary

Two series of nanocomposites from the $Fe_xO_y$–$SiO_2$ system, containing 20 mass% iron oxide were prepared by the alkoxide route of the sol–gel method, in the absence and presence of catalyst. The silica gel has been obtained using tetraethoxysilane. The iron(III) nitrate nonahydrate has been used as iron oxides source. The samples have been prepared in identical conditions, differing only by the gelation times, induced by different surface of evaporation/volume (*S*/*V*) ratios of sol let to gelify. Thermal analysis data have established the thermal treatments conditions of the prepared samples and were correlated with X-ray diffraction, IR spectroscopy and TEM results, in order to accomplish a complete structural characterization. The correlation between the structural modifications of the $Fe_xO_y$–$SiO_2$ nanocomposites and different conditions of drying has been established.

***Keywords:*** *iron-silica nanocomposites, sol–gel method, thermal analysis*

## Introduction

The synthesis of materials in the nanometer range is a subject of great interest due to their distinct chemical, magnetic and optical properties. Among the various preparation procedures of nanocomposites, the sol–gel method offers some special advantages. It allows the control of the final properties of the material and represents an effective remedy to the tendency of nanopowders to aggregate, ensuring the homogeneous dispersion of some ultra-fine metal oxide particles in the host matrix.

Concerning the sol–gel iron-silica nanocomposites, the material consists of a $SiO_2$ matrix which contains one of the polymorphs of the iron(III) oxide: $\alpha$-$Fe_2O_3$ (hematite), $\gamma$-$Fe_2O_3$ (maghemite), $\varepsilon$-$Fe_2O_3$, $\beta$-$Fe_2O_3$ or amorphous $Fe_2O_3$ [1–8]. Hematite ($\alpha$-$Fe_2O_3$), the antiferromagnetic hexagonal form, represents the most thermodynamically stable polymorph of the iron(III) oxides, so it is easiest to be obtained. However, the most studied polymorph remains maghemite ($\gamma$-$Fe_2O_3$), the ferromagnetic cubic form [5, 6, 9, 10], due to its magnetic properties, which ensure many technological applications. Its obtaining is difficult because of the $\gamma$- to $\alpha$-$Fe_2O_3$ transition, which is not easy to be controlled. The explanation consists in the multitude of factors that can affect the stability of iron oxides. Therefore, the reported transition temperatures ($T_{\gamma\rightarrow\alpha}$) vary in the range 300–600°C [11], even higher than 650°C [9]. $\varepsilon$-$Fe_2O_3$, the ferromagnetic orthorhombic form is a rare polymorph, difficult to synthesize as single-phase, but typically obtained as mixtures of $\varepsilon$- plus $\alpha$- and/or $\gamma$-$Fe_2O_3$ [7, 8]. Depending on the iron precursor used and on the process parameters of the sol–gel synthesis, besides all these polymorphs of the iron(III) oxide, a series of iron oxyhydroxides, such as goethite: $\alpha$-FeO(OH) and lepidocrocite: $\gamma$-FeO(OH) or fayalite ($Fe_2(SiO_4)$, can be obtained.

The authors of the present paper have recently studied the obtaining of $Fe_3O_4$–$SiO_2$ nanocomposites via alkoxide and colloidal route of the sol–gel method [12]. They put in evidence the influence of the type of silica matrix on the structure, size and distribution of the $Fe_3O_4$ nanoparticles in these nanocomposites with magnetic properties.

The properties of the final nanocomposite are mainly determined by the sol–gel parameters, referring both to the chemical composition, and to the reaction conditions: the metal and silica precursors, their concentrations, the molar ratios between components, the nature of the catalyst, the pH and temperature values. Another parameter which is very important for the final properties of the obtained

* Author for correspondence: abrail@icf.ro

*1388–6150/$20.00*

*Akadémiai Kiadó, Budapest, Hungary*
*Springer, Dordrecht, The Netherlands*

nanocomposites consists in the drying conditions, which can be varied through the control of the surface of evaporation/volume (*S*/*V*) ratios of sol let to gelify.

All the mentioned factors have a major influence on the particle size, the size distribution and the iron oxide phase formed in the final nanocomposite. As Piccaluga *et al.* [13] have already mentioned, because of the extremely high number of variables which influence the method, the results reported in the literature are not easy to be compared.

In the present work, from the multitude of sol–gel parameters influencing the iron oxide phase obtained in the final nanocomposite, those related to the drying conditions have been chosen.

The paper has studied two series of nanocomposites from the $Fe_xO_y$–$SiO_2$ system, containing 20 mass% $Fe_2O_3$ (related to $SiO_2$), prepared by the alkoxide route of the sol–gel method, differing by the absence or presence of catalyst in the synthesis. Both series of samples have been prepared in identical conditions, differing only by the gelation times, induced by different surface of evaporation/volume (*S*/*V*) ratios of the sols. The modifications induced in the prepared nanocomposites by changing the mentioned sol–gel parameters have been studied mainly with the aid of thermal analysis, whose results have been sustained by XRD, IR and TEM measurements. The mentioned methods have been also used for the characterization of other types of nanocomposites [14].

## Experimental

### *Samples preparation*

Two series of sol–gel $Fe_xO_y$–$SiO_2$ nanocomposites containing 20 mass% $Fe_2O_3$ related to $SiO_2$ have been prepared, in identical synthesis conditions. The only difference between them consisted in the absence (series A) or presence (series B) of HCl addition, as catalyst. The silica precursor was tetraethylorthosilicate (TEOS) and the $Fe_xO_y$ source was the iron(III) nitrate nonahydrate ($Fe(NO_3)_3{\cdot}9H_2O$), both reagents from Merck. The solvent used in the sol–gel reaction for the TEOS alkoxide was $C_2H_5OH$ from Riedel de Häen.

An appropriate quantity of EtOH was used in order to dissolve the iron(III) nitrate nonahydrate, by stirring at the room temperature. After the total dissolution of the salt, the ethanolic solution was poured, drop by drop, in a mixture of TEOS and EtOH, under vigorous stirring, also at the room temperature. The molar ratio between alkoxide and solvent was TEOS:EtOH=1:16. Concerning the quantity of water necessary for promoting the hydrolysis reaction, for series A it has been proceeded only from the hydration water of the iron salt. For series B, a supplementary quantity of water has been added together with the acid catalyst, introduced in the reaction mixture as last step of the sol–gel preparation.

Both sols, corresponding to series A and B, have been stirred for 30 min, at room temperature. Then, each of them was poured into three identical vessels, differing one from the other only through the quantity of sol content. The six resulted samples were covered with watch glasses and let to gelify in an oven at 50°C. The different volumes of sols let to gelify in identical vessels, which correspond to different surface of evaporation/volume of sol ratios led to different gelation times of the prepared nanocomposites. Table 1 presents this correspondence, together with the codification of samples.

Both silica matrices (m-$M_{30}$ and m-$M_{30+A}$) have been obtained in identical conditions with the corresponding nanocomposites, eliminating only the addition of $Fe(NO_3)_3{\cdot}9H_2O$ from the reaction mixture.

**Table 1** The gelation conditions and the gelation times of the prepared nanocomposites

| Series | Sample* | *S*/*V*/ $mm^{-1}$ | pH | *T*/ °C | Gel. time/ day |
|---|---|---|---|---|---|
| A | $M_{10}$ | 0.08 | ≈4 | 50 | 1.5 |
| | $M_{20}$ | 0.04 | | | 3.5 |
| | $M_{30}$ | 0.03 | | | 8.0 |
| | m-$M_{30}$ | 0.03 | | | >30 |
| B | $M_{10+A}$ | 0.08 | ≈3 | 50 | 2.0 |
| | $M_{20+A}$ | 0.04 | | | 4.0 |
| | $M_{30+A}$ | 0.03 | | | 10.0 |
| | m-$M_{30+A}$ | 0.03 | | | 5.5 |

*The inferior index (10, 20, 30) indicates the number of mL of sol corresponding to each sample; the presence of letter 'A' at the inferior index indicates the samples belonging to series B, in whose preparation an acid catalyst was used; m-$M_{30}$ represents the silica matrix corresponding to sample $M_{30}$; m-$M_{30+A}$ represents the silica matrix corresponding to sample $M_{30+A}$

### *Samples characterization*

The prepared nanocomposites were characterized by:

- Thermal analysis, performed up to 700°C using a STD 2960 simultaneous TG-DTG-DTA apparatus (TA Instruments); heating rate 10 K $min^{-1}$, flowing air and $N_2$ atmosphere; 130 mL $min^{-1}$;
- X-ray diffraction, using a computer controlled DRON DART UM-2 diffractometer equipped with a $CuK_\alpha$ source and a graphite monochromator in the diffracted beam (the scanning technique was applied with a step width of 0.05° and an acquisition time on each step of 2 s, ranging from 2θ=15–67°).

- IR spectroscopy, in the 4000–400 $cm^{-1}$ range, with a Carl Zeiss Jena Specord 80 Spectrophotometer.
- Transmission electron microscopy (TEM), collecting images with a JEOL 200 CX.

## Results and discussion

Before presenting the results regarding the characterization of the prepared nanocomposites, a few specifications concerning the sol–gel method are important to be done.

Although the sol–gel preparation can proceed with a wide variety of precursors, most literature results are based on the alkoxidic approach. In these conditions, the sol–gel chemistry can be described in terms of two types of reactions, starting from alkoxidic precursor (TEOS): hydrolysis reactions (1)–(4):

$$Si(OC_2H_5)_4 + H_2O \leftrightarrow HO–Si(OC_2H_5)_3 + C_2H_5OH \quad (1)$$

$$HO–Si(OC_2H_5)_3 + H_2O \leftrightarrow (OH)_2Si(OC_2H_5)_2 + C_2H_5OH \quad (2)$$

$$(OH)_2Si(OC_2H_5)_2 + H_2O \leftrightarrow (OH)_3Si(OC_2H_5) + C_2H_5OH \quad (3)$$

$$(OH)_3Si(OC_2H_5) + H_2O \leftrightarrow Si(OH)_4 + C_2H_5OH \quad (4)$$

and condensation reactions (5) and (6):

$$\equiv Si–OC_2H_5 + HO–Si\equiv \leftrightarrow \equiv Si–O–Si\equiv + C_2H_5OH \quad (5)$$

$$\equiv Si–OH + HO–Si\equiv \leftrightarrow \equiv Si–O–Si\equiv + HOH \quad (6)$$

The hydrolysis occurs when the alkoxide and water are mixed, using an alcohol as solvent. The reaction can proceed in acidic or basic conditions.

Despite this oversimplification (both types of reactions occur almost simultaneously and generally are not completed), this description of the sol–gel chemistry implies two key ideas. First, a gel forms because of the condensation of partially hydrolyzed species into a three-dimensional polymeric network. Second, any factors that affect either one or both types of these reactions are likely to impact on the properties of the resulted gel.

Depending on the relative kinetics of the hydrolysis and condensation reactions it is possible to obtain either linear polymers, or colloidal dense particles or intermediate, consisting from agglomerates of weak reticulated polymers. For the case of TEOS, Pierre [15] makes the distinction between the progress of the gelation process in acidic-, respectively alkaline-catalyzed conditions. He considers that the acid-catalyzed conditions correspond to a pH<2.5 and in all cases the hydrolysis controls the process more than condensation. At pH values >2.5 Pierre speaks about the alkaline-catalyzed gelation, in which case the condensation reactions are determinant. If, yet, the acidity becomes strong enough, the smallest polymers can depolymerize in the same time with the growth of the biggest ones. Thus, although the condensation is faster than hydrolysis, it can be attenuated by depolymerizing. These could explain the fact that, although catalyzed, the samples from series B have gelified slower than the corresponding ones belonging to series A, obtained in the absence of catalyst, as it can be seen from Table 1.

Concerning the gelation time of the prepared samples, another observation resulted from data of Table 1 refers to its dependence on the evaporation surface to volume ratio of sol: as expected, for both series of iron-silica nanocomposites (A and B) it increases as $S/V$ parameter decreases, according to a slower evaporation of the solvent.

### *Thermal analysis*

Thermal analysis is a very suitable method for the characterization of the amorphous phases obtained by the sol–gel method.

### *Series A*

TG-DTG-DTA curves of the dried gels $M_{20}$ and $M_{30}$ obtained in flowing air atmosphere are quite similar. Fig-

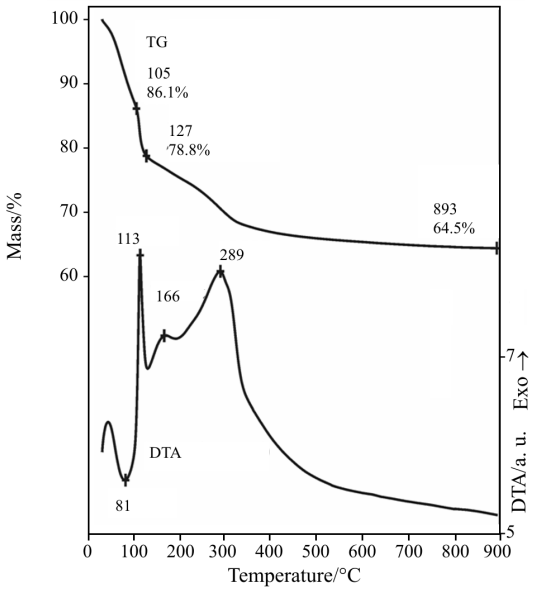


**Fig. 1** Thermal behaviour of the dried gel $M_{30}$, in flowing air atmosphere. Initial mass 12.39 mg

ure 1 represents the thermal behaviour of the sample $M_{30}$.

Under 100°C (86, respectively 81°C), an endothermic peak, assigned to the loss of the alcohol and adsorbed water, can be observed. The iron nitrate decomposition is evidenced by a sharp exothermic peak (much more pronounced for the sample $M_{30}$) at ~100°C (106 and 113°C, respectively). This one overlaps with a broad exothermic peak (with two maxima), associated with the combustion of the organic species from the silica matrix. The final residue of samples $M_{20}$ and $M_{30}$ at around 900°C is 67.3 and 64.5%, respectively.

The thermal behaviour of the sample $M_{30}$ in nitrogen atmosphere presents the low temperature endothermic effect (81°C) and the sharp exothermic peak (113°C), too. The final residue of sample $M_{30}$ in flowing $N_2$ at around 900°C is 69.2%.

*Series B*

The thermal behaviour of the silica matrix corresponding to the composition $M_{30+A}$, in $N_2$ atmosphere, is that of a common xerogel, with a major mass loss associated with the endothermic effect at 87°C (Fig. 2).

TG-DTG-DTA curves of the dried gels $M_{20+A}$ and $M_{30+A}$ in flowing air atmosphere are rather similar. Figure 3 presents the thermal behaviour of the sample $M_{30+A}$. The presence of the acid catalyst in the reaction mixture changes the aspect of the DTA curves. The low temperature endothermic peak under

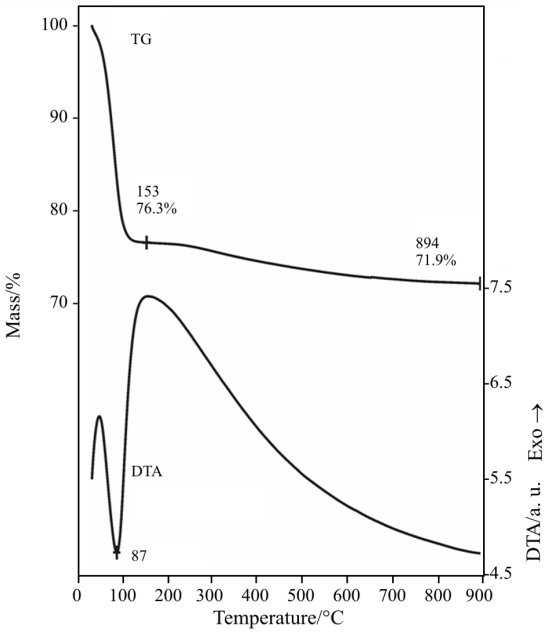


**Fig. 2** Thermal behaviour of the silica matrix corresponding to the dried gel $M_{30+A}$, m-$M_{30+A}$, in flowing $N_2$ atmosphere. Initial mass 11.06 mg

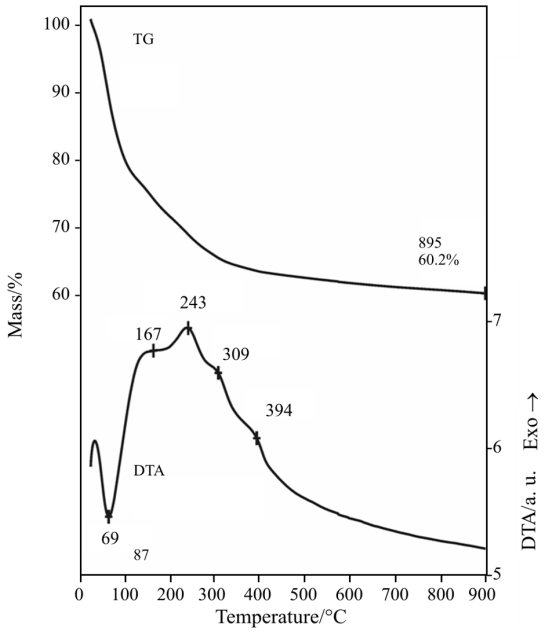


**Fig. 3** Thermal behaviour of the dried gel $M_{30+A}$, in flowing air atmosphere. Initial mass 10.63 mg

100°C is present on the DTA curves, but the sharp exothermic one due to the Fe(III) nitrate decomposition vanishes. This can be explained by the reaction between $Fe(NO_3)_3 \cdot 9H_2O$ and HCl which determines a different gelation mechanism. This fact is sustained by the different aspect of the DTG curves, which accounts for several successive decomposition steps compared to the samples belonging to series A, 3 and 4 for sample $M_{20+A}$ and $M_{30+A}$, respectively. These ones are associated with corresponding effects on the broad DTA exothermic peak, probably due to the decomposition and burning out of organic residues. The final residue of samples $M_{20+A}$ and $M_{30+A}$ at around 900°C is 64.8 and 60.2%, respectively.

The thermal behaviour of the sample $M_{30+A}$ in nitrogen atmosphere shows the effect of the catalyst on the gelation mechanism (the presence of one supplementary step on DTG curve), too. The final residue of sample $M_{30+A}$ in flowing $N_2$ at around 900°C is 63.4%.

*IR spectroscopy results*

The IR vibration bands of the prepared nanocomposites are presented in Table 2, for both cases: before and after the thermal treatment, performed at 400°C, for 4 h.

As it can be seen from Table 2, both series of samples (A and B) present the typical absorption bands for a silica matrix resulted from a TEOS precursor, together with the absorption bands which put in evidence the presence of the incorporated iron in the

**Table 2** IR vibration bands of the prepared nanocomposites: un-treated (un-t) and thermally treated at 400°C for 4 h (tt)

| $\nu/cm^{-1}$ | | | | | | | | | Assignment |
|---|---|---|---|---|---|---|---|---|---|
| Series A | | | | | Series B | | | | |
| $M_{10}$ | $M_{20}$ | | $M_{30}$ | | $M_{10+A}$ | $M_{20+A}$ | | $M_{30+A}$ | |
| tt | un-t | tt | un-t | tt | tt | un-t | tt | un-t | |
| 3425 | 3450 | 3425 | 3450 | 3450 | 3400 | 3450 | 3425 | 3450 | structural $OH^-$ |
| 1650 | 1640 | 1650 | 1650 | 1650 | 1630 | 1650 | 1650 | 1650 | $\delta_{HOH}$ |
| – | 1390 | – | 1380 (s) | – | – | 1400 (w) | 1400 (w) | 1400 (w) | $\nu_{NO_3^-}$ |
| 1150 | 1070 | 1100 | 1070 | 1100 | 1125 | 1180 | 1100 | 1070 | $\nu_{as(Si–O–Si)}$ |
| 950 (w) | – | 940 | 940 | – | 950 (w) | 950 | – | 950 (w) | $\nu_{s(Si–OH)}$ |
| 800 (w) | 800 (w) | 780 (w) | 780 (w) | 720 (w) | 800 (w) | 750 (w) | 800 (w) | 750 (w) | $\nu_{s(Si–O–Si)}$ |
| 550 | – | – | – | – | 550 | – | – | – | $\nu_{Fe–O}$ |
| 545 | – | – | – | – | 545 | – | – | – | Si–O–Si from cyclic tetramers |
| 460 (w) | – | – | – | – | 460 (w) | – | – | – | $\delta_{O–Si–O}$ |
| 500–400 | 500–400 | 500–400 | 500–400 | 500–400 | 500–400 | 500–400 | 500–400 | 500–400 | $\nu_{Fe–O}$ |

mentioned matrix at 550 $cm^{-1}$ in accordance with Bruni *et al.* [16].

The presence of the vibration band at 1390, respectively 1380 $cm^{-1}$ in the spectra of the untreated samples from series A, evidences the existence of the unreacted residual ethoxy groups in the silica matrix, which disappear from the IR spectra of the corresponding thermally treated samples. Concerning the nanocomposites from series B, this band (slightly shifted to 1400 $cm^{-1}$) is much weaker than in the series A case. This can be explained by the presence of catalyst in the reaction mixture, which favours the hydrolysis *vs.* polycondensation reactions (less unreacted ethoxy groups from TEOS precursor). Thermal analysis results of the B series samples pointed out the iron nitrate decomposition and consequently the 1400 $cm^{-1}$ band can be assigned to $NO_3^-$ vibration. Another interesting observation from the IR determinations refers to the samples $M_{10}$, respectively $M_{10+A}$, with the same and biggest *S*/*V* ratio (0.08). It seems that the presence of the vibration band at 545 $cm^{-1}$ evidences the fact that the gelation occurs through some cyclic intermediaries.

*X-ray diffraction results*

The XRD data obtained for the prepared iron-silica nanocomposites thermally treated at 400°C for 4 h are presented in Figs 4a and b.

As it can be seen from Fig. 4a, corresponding to the series of samples obtained in the absence of catalyst (series A), no matter the evaporation conditions (*S*/*V* of sol ratio), the materials exhibit a typical pattern of an amorphous, with extremely small particles. The amorphous character can be the result of either a very disordered structure or of a so small crystallite size as to escape observation by XRD. However, the drying conditions influence slightly the crystallization process of particles, being observable a progressive decrease of particle size with increasing *S*/*V* from 0.03 (corresponding to sample $M_{30}$ which is the most crystallized from the series A) to 0.08 (corresponding to sample $M_{10}$ which is the most amorphous). The fact that as the *S*/*V* of sol ratio increases, the XRD peaks become indistinguishable from the amorphous silica background is confirmed by the literature data [5, 6, 9, 17]. The presented patterns from Fig. 4a display a predominant very broad peak at around $2\theta=21°$ and some very poorly defined peaks. The predominant amorphous peak position corresponds to the most intense peak (110) of the FeO(OH)–goethite phase and the ascription of the others poorly-defined peaks to the FeO(OH)–goethite phase could be tentatively proposed.

Concerning Fig. 4b, which presents the XRD spectra corresponding to samples belonging to series B (obtained in the presence of acid catalyst), beside the goethite phase the formation of the spinelic $\gamma$-$Fe_2O_3/Fe_3O_4$ oxide phase can be observed, no matter of the value of the *S*/*V* ratio. Figure 4b shows also the fact that as the *S*/*V* ratio decreases (respectively the gelation time increases), the presence of the mentioned oxide phase is more evident (sample $M_{30+A}$). According to the literature data [18] it is possible that

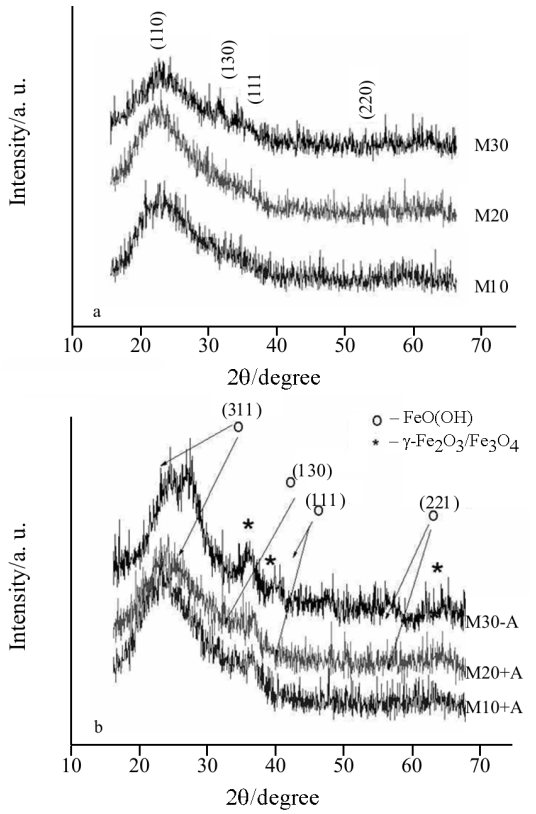


**Fig. 4** XRD spectra of the prepared samples, obtained in a – the absence and b – the presence of catalyst, thermally treated at 400°C/4 h

the iron oxide-hydroxide polymers nucleated in the silica pores to be responsible for the spinelic $\gamma$-$Fe_2O_3/Fe_3O_4$ phase, presumed to be formed in the sample $M_{30+A}$ submitted to 400°C.

The XRD results confirm the existing differences between samples belonging to series A and B, also established by the thermal analysis.

*TEM results*

The TEM images are in agreement with the XRD results, putting in evidence the amorphous character of the prepared samples. The only exceptions are represented by the $M_{30}$, respectively $M_{30+A}$ samples, obtained with the same lowest *S*/*V* ratio of sol (0.03). Figures 5 and 6 present the obtained TEM images of the sample $M_{30}$ before and after thermal treatment.

It can be seen that before the thermal treatment the structure is amorphous. Then, some of precipitates remain probably still amorphous but the rest are partially crystallized. They appear as weakly facetated, having sizes of 3 to 25 nm. The very small number of crystalline nanoparticles evidenced by the TEM images is in agreement with the literature information [9].

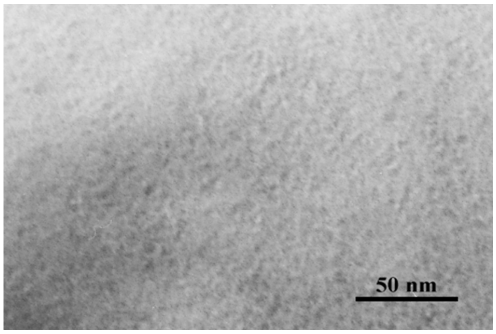


**Fig. 5** TEM image of the sample $M_{30}$, not thermally treated

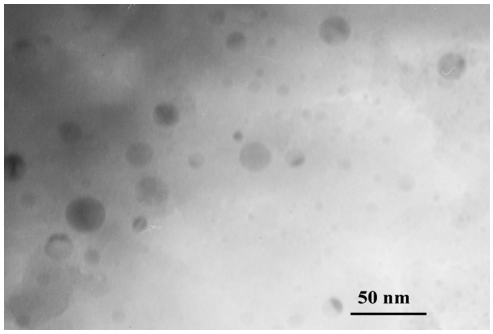


**Fig. 6** TEM image of the sample $M_{30}$, thermally treated at 400°C/4 h

## Conclusions

Two series of iron-silica nanocomposites containing 20 mass% $Fe_2O_3$ (related to $SiO_2$) have been prepared by the alkoxide route of the sol–gel method differing by the absence (series A) or presence of catalyst in the synthesis (series B).

The evaporation conditions and as a consequence the gelation times have been varied for both series through the control of the surface/volume ratio of the sol (*S*/*V*). It was established that these conditions influence the final properties of the prepared nanomaterial.

The modifications induced by changing the mentioned sol–gel parameters have been studied with the aid of thermal analysis, whose results have been sustained by XRD, IR and TEM determinations.

The gelation times of samples obtained in the presence of catalyst are longer than those corresponding to the uncatalyzed samples.

The X-ray diffraction and transmission electron microscopy analyses of samples indicated a variation of the particles size, in a reverse proportional relation with the *S*/*V* ratio (respectively directly proportional with the gelation time). Samples $M_{30}$ respectively $M_{30+A}$ present the biggest particles.

The formation of some chemical compounds is possible to be assumed, which is suggested by XRD and confirmed by the DTA measurements. The nanocomposites obtained in the absence of catalyst are

amorphous, only for the lowest $S/V$ value (sample $M_{30}$) presenting a weak tendency of crystallization (the goethite phase). In the presence of catalyst, no matter of the $S/V$ ratio of sol, beside the goethite, an oxide phase is also present (the spinelic $\gamma$-$Fe_2O_3/Fe_3O_4$ one). Its diffraction lines are the most evident for sample $M_{30+A}$.

## Acknowledgements

The authors are grateful to Mr. V. S. Teodorescu, Ph.D. at the National Institute for Physics of Materials (Bucharest, Roumania), for performing the TEM analysis and for his helpful suggestions.

## References

1 T. López, J. Méndez, T. Zamudio and M. Villa, Mater. Chem. Phys., 30 (1992) 161.
2 A. Jitianu, M. Crişan, A. Meghea, I. Rău and M. Zaharescu, J. Mater. Chem., 12 (2002) 1401.
3 M. Răileanu, M. Crişan, C. Petrache, D. Crişan and M. Zaharescu, J. Optoelectron. Adv. Mater., 5 (2003) 693.
4 J. P. Jolivet, E. Tronc and C. Chanéac, Eur. Phys. J., AP 10 (2000) 167.
5 S. Solinas, G. Piccaluga, M. P. Morales and C. J. Serna, Acta Mater., 49 (2001) 2805.
6 C. Cannas, G. Concas, D. Gatteschi, A. Musinu, G. Piccaluga and C.Sangregorio, J. Mater. Chem., 12 (2002) 3141.
7 C. Chanéac, E. Tronc and J. P. Jolivet, Nanostruct. Mater., 6 (1995) 715.
8 M. Popovici, M. Gich, D. Nižňansky, A. Roig, C. Savii, L. Casas, E. Molins, K. Zaveta, C. Enache, J. Sort, S. deBrion, G. Chouteau and J. Nogués, Chem. Mater., 16 (2004) 5542.
9 G. Ennas, A. Musinu, G. Piccaluga, D. Zedda, D. Gatteshi, C. Sangregorio, J. L. Stanger, G. Concas and G. Spano, Chem. Mater., 10 (1998) 495.
10 F. del Monte, M. P. Morales, D. Levy, A. Fernandez, M. Ocaña, A. Roig, E. Molins, K. O'Grady and C. J. Serna, Langmuir, 13 (1997) 3627.
11 G. Ennas, G. Marongiu, A. Musinu, A. Falqui, P. Ballirano and R. Caminiti, J. Mater. Res., 14 (1999) 1570.
12 A. Jitianu, M. Răileanu, M. Crişan, D. Predoi, M. Jitianu, L. Stanciu and M. Zaharescu, J. Sol–Gel Sci. Technol., 40 (2006) 317.
13 G. Piccaluga, A. Corrias, G. Ennas and A. Musinu, Mater. Sci. Foundations, 13 (2000) 4.
14 S. C. Mojumdar and L. Raki, J. Therm. Anal. Cal., 85 (2006) 99.
15 A. C. Pierre, Introduction aux procédés sol-gel, Éditions SEPTIMA, Paris 1992, p. 25.
16 S. Bruni, F. Cariati, M. Casu, A. Lai, A. Musinu, G. Piccaluga and S. Solinas, Nanostruct. Mater., 11 (1999) 573.
17 C. Cannas, G. Concas, F. Congiu, A. Musinu, G. Piccaluga and G. Spano, Z. Naturforsch., 57a (2002) 154.
18 G. Ennas, M. F. Casula, G. Piccaluga, S. Solinas, M. P. Morales and C. J. Serna, J. Mater. Res., 17 (2002) 590.

DOI: 10.1007/s10973-006-8124-y